J Solid State Electrochem (2010) 14:1787–1792
DOI 10.1007/s10008-010-1012-1

ORIGINAL PAPER

Lithium ion pathways in $LiFePO_4$ and related olivines

Stefan Adams

Received: 18 November 2009 / Revised: 12 January 2010 / Accepted: 17 January 2010 / Published online: 9 February 2010

Abstract Determining ion transport pathways as regions of low bond valence mismatch represents a simple, reliable way of characterizing ion transport pathways in local structure models, provided that the local structure model captures the essential structural features. The examples of $LiFePO_4$ and other olivine-type mixed conductors discussed here demonstrate the impact of structural disorder on the ion transport pathway and mechanism. The effect of Li'_{Fe} antisite defects on the transition from one- to two-dimensional conduction pathway dimensionality as well the possibility of heterogeneous doping of $LiFePO_4$ by a lithium phosphate glass surface layer are discussed in detail.

Keywords Lithium ion batteries · Nanostructured energy storage materials · Heterogeneous doping · Molecular dynamics simulation · $LiFePO_4$ electrodes

Introduction

It is well established by a variety of computational techniques [1–4] that Li^+ ion transport in the ordered structure of $LiFePO_4$ [5, 6] follows a zigzag-shaped one-dimensional pathway along the *b* direction. Yet experimental data on pure and doped single crystals suggest that the low Li^+ ion conductivity in $LiFePO_4$ is practically two-dimensional within the *b*–*c* plane [7, 8], while other single-crystal measurements [9] are consistent with the expected one-dimensional migration. Obviously, structural disorder may affect both the value and the anisotropy of the rate-limiting ionic diffusion coefficient. In contrast to experimental measurements, bond valence (BV) pathway models—applied in this work to local structure models from molecular dynamics (MD) simulations—do not require special procedures for treating mixed conductors, as the orders of magnitude faster electronic conduction processes will hardly affect the modeling for cation conductors (except for slight changes of repulsions between lithium and immobile cations). Moreover, Kang and Ceder recently demonstrated extraordinarily high discharge rates of Li batteries based on $LiFePO_4$ with a "fast ion-conducting surface phase through controlled off-stoichiometry" [10]. Here, we discuss a possible mechanism of enhanced ion migration assuming that these samples actually contain $LiFePO_4$ surface modified by glassy $Li_4P_2O_7$ combining MD simulations with a BV analysis of the resulting structure models. This study, therefore, aims to clarify the effect of (a) intrinsic antisite defects and (b) surface modifications on the static and dynamic Li^+ distribution and the dimensionality of Li^+ ion mobility.

Experimental

The modeling of pathways for mobile Li^+ as regions of low site energy E(Li) (or of low BV sum mismatch $|\Delta V$(Li)|) has been demonstrated to be a simple and reliable way of characterizing transport pathways in local structure models, provided that the local structure model captures the essential structural features [4, 11]. While BV $s_{Li-O} = \exp[(R_0 - R)/b]$ and hence the BV sum mismatch $|\Delta V|$ are usually expressed in arbitrary "valence units," they can—

S. Adams (✉)
Department of Materials Science and Engineering,
National University of Singapore,
7 Engineering Drive 1, E3A #04-02,
Singapore 117574, Singapore
e-mail: mseasn@nus.edu.sg

as we have recently shown—be linked to an absolute energy scale by expressing the BV as a Morse-type interaction energy:

$$E(\mathrm{Li}) = D_0\left[\sum_{i=1}^{N}\left(\frac{s_{\mathrm{Li-O}} - s_{\min \mathrm{Li-O}}}{s_{\min \mathrm{Li-O}}}\right)^2 - N\right] + E_{\mathrm{Coulomb}}(\mathrm{Li-Fe}). \quad (1)$$

For details, see ref. [11]. Note that, for the analysis of E(Li) or ΔV(Li), Coulomb repulsions are considered only between mobile and immobile cations (i.e., here between Li^+ and Fe^{2+}). The same empirical BV parameters s_{A-X}, $R_0(A-X)$ used in this pathway analysis are also used as force field parameters for the generation of disordered local structure models by MD simulation, yet of course including all Coulomb repulsions, as done in this work for the first time.

MD simulations of bulk $Li_{0.99}FePO_4$ with a single built-in $Li'_{Fe}/Fe^{\bullet}_{Li}$ antisite defect and one lithium vacancy per 96 formula units, of bulk $Li_4P_2O_7$ glass $[(Li_2O)_{0.667}(P_2O_5)_{0.333}]_{491}$ and of a 4,367-atom 3D-periodic $LiFePO_4$:$Li_4P_2O_7$ interface structure ($43\times62\times21$ Å^3) have been conducted using the software GULP [12] as implemented in Materials Studio 4.4 [13]. Attractive interactions were treated by the Morse-type term in Eq. 1 using the BV parameters of our *softBV* parameter set [14]. In contrast to the pathway modeling, Coulomb cation–cation and anion–anion repulsions have been considered for all atom types with fractional charges chosen to be 0.83 times the formal charges and an erfc-type screening function. The extra (fractional) charge due to the deviation of the Li content from unity is equally distributed over all iron cations to emulate a charge transfer on a time scale that is faster than that of ionic transport. Production runs were extended over 1,500 ps for T=500–1,000 K, 9,000 ps for T=450 K, and 10,000 ps for T=400 K.

For bulk $Li_{0.99}FePO_4$, the chosen structure model with one built-in antisite defect permits to quantify Li^+ diffusion only along the channel direction ($\|b$). The run at T=400 K is not discussed further, as it did not yield a clearly quantifiable slope of the mean square displacement vs. time curve. The contact surface for the $LiFePO_4$:$Li_4P_2O_7$ heterostructures is chosen to be (010) as it is the most prominent surface of $LiFePO_4$ nanoparticles and provides access to the Li^+ transport cannels along the b direction. For the heterostructures, a 750-ps equilibration before the first production run (or 150 ps in-between runs at different temperatures) was followed by 600 ps (for T=600–1,000 K), 1 ns (for T=500 K), or 3 ns (for T=300–400 K) production runs.

Monte Carlo simulations have been performed for a 180 $b\times180$ c supercell of the Li substructure of $LiFePO_4$ structure to identify the percolation threshold for two-dimensional mobility in the b–c plane with varying energy penalties for the degree of correlation between the location of the $Fe^{\bullet}_{Li}$ and the Li'_{Fe} of a single antisite pair as well as the correlation between the locations of different antisite pairs, while the number of antisite defects tends to be increased until two-dimensional percolation is achieved. Simulation results were averaged over 1,000 runs for each setting.

Results and discussion

Static bond valence pathway models

BV pathway models for the average (fully ordered) crystal structure [5, 6] obviously agree with ab initio calculations in predicting a zigzag-shaped one-dimensional pathway for the Li ions along the b direction (cf. Fig. 1a, b). Since some experimental data [7, 8] suggest that the Li^+ conductivity is

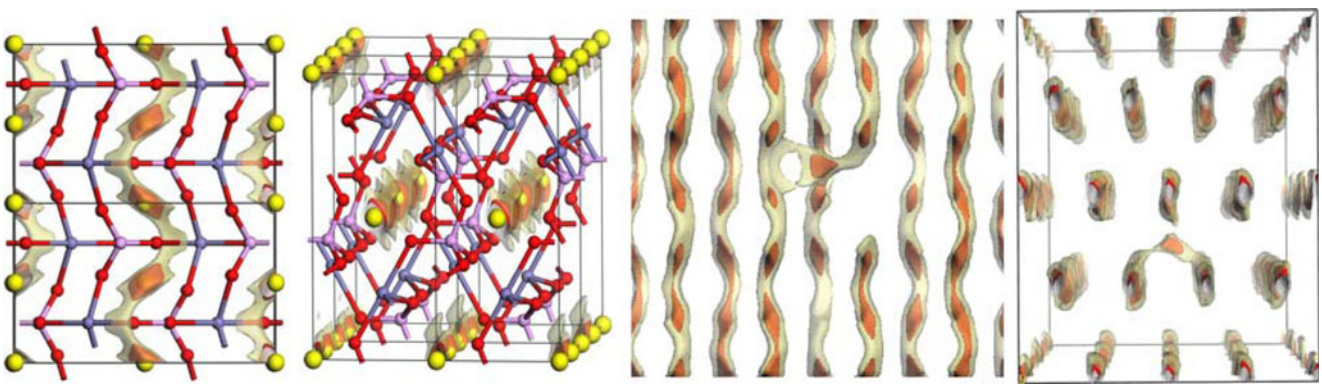

Fig. 1 BV model of one-dimensional zigzag Li^+ pathways in the fully ordered $LiFePO_4$ structure projected on **a** a–b plane and **b** approximate a–c plane (Li sites: *large light spheres*). Changes in the pathways caused by a single $Li'_{Fe}/Fe^{\bullet}_{Li}$ antisite pair are demonstrated in projections **c** on the b–c plane and **d** on the a–c plane. *Light* (*dark*) isosurfaces correspond to BV site energies characteristic for long-range migration (local vibrations)

practically two-dimensional within the *b*–*c* plane, while other experiments yield an ion transport preferentially along the channel direction [9], here, we investigate whether a more detailed structure model that includes likely defect scenarios affects the pathway prediction. Of particular importance is the occurrence of Li^{+}/Fe^{2+} antisite defects [1]. Again, simple BV calculations may be used as a quick check on the plausibility of antisite defects. Fe^{2+} on a Li^{+} site in the structure gets exactly the matching BV sum $V(Fe_{Li})=2$ as on its equilibrium site and the BV sum for a Li on a Fe site is $V(LiFe)=1.0$. An energetic disadvantage, however, arises from the effect on the BV sums of the surrounding oxygen atoms. The global instability index (GII), i.e., the root mean square BV sum mismatch averaged over all distinct atoms in the $LiFePO_4$ structure would rise from GII=0.035 for the ordered crystal structure (based on literature structure data [5, 6]) to GII=0.103 for a hypothetical structure where Li and Fe are completely exchanged. Accordingly, Fisher et al. [15] find a moderate energetic disadvantage of antisite defects (1.1 eV). This indicates that antisite defects will occur even in fully equilibrated samples, but major concentration variations are to be expected due to the commonly applied sample preparation routes under nonequilibrium conditions (Rietveld refinements in [16–18] suggest up to 6–8% $Fe^{\bullet}_{Li}$ in as-prepared $LiFePO_4$ grown by low-temperature hydrothermal methods, but the defect concentration is reduced substantially by subsequent thermal annealing). Recently, antisite defects in $LiFePO_4$ could also be directly visualized by scanning transmission electron microscopy (TEM) [19]. As seen from BV pathway models in Fig. 1c, d for a model containing a single antisite pair, its effect on the local pathways is twofold: $Fe^{\bullet}_{Li}$ inside the pathway channel blocks the channel along *b*, while Li'_{Fe} represents a new connection between channels perpendicular to the *b* direction.

Monte Carlo simulations

To achieve a percolating two-dimensional pathway, a sufficient number of such defects is required. From Monte Carlo simulations in a 180×180 Li site supercell with periodic boundary conditions (to model bulk behavior), the concentration of antisite defects necessary to create a percolating Li pathway cluster (that spans the simulated cell in both *b* and *c* directions) is estimated to be approximately 4.6% as long as no correlation between the positions of antisite pairs is assumed. This percentage is practically independent of whether it is supposed that the antisite pair ions remain immediate neighbors or their positions are independent of each other. Anyway, during delithiation, the Li'_{Fe} as a higher energy site will be preferentially vacated [16, 17, 20], but again, the blocking of channels by the iron cation and the connection of channels by the missing iron cation will persist. Introducing a significant energetic preference for the formation of antisite defects in the vicinity of existing defects reduces the minimum percolation threshold to about 2.2%. While—as mentioned above—defect concentrations will strongly depend on the thermal history and stoichiometry, estimates from X-ray and neutron diffraction for preannealed materials are typically around 2%. TEM visualizations also qualitatively suggest that the antisite defects are not randomly distributed but to some extent clustered [16, 17]. It may, therefore, be tentatively concluded that experimental observations of two-dimensional Li^{+} mobility and of TEM observations are consistent. Defect concentrations required for a long-range two-dimensional Li mobility may preferentially be reached by synthesis routes that prevent equilibration. It should, however, be kept in mind that the reduced anisotropy of the lithium mobility is partially achieved by reducing the mobility along the channels, so that a higher pathway dimensionality should not be uncritically identified with a faster transport. More detailed structure models will be required to determine the effect of particle size, delithiation (V'_{Li} compensated by $Fe^{\bullet}_{Fe}$) as well as of other aliovalent dopants on the percolation threshold.

Generalization to $LiMPO_4$

Since it is found that the antisite defect concentration can play a critical role for the dimensionality of the ion transport pathways in this structure, it has also been investigated how a partial or total replacement of Fe^{2+} by other divalent transition metal cations would affect the antisite pair concentration $c_{antisite}$. For the range of cations covered in Fig. 2, all ions except Co^{2+} lead to significantly higher BV mismatches for antisite pairs and, therefore, reduced values of $c_{antisite}$. Thus, it is not to be expected that any $LiMPO_4$ olivine except for the series $LiFe_{1-x}Co_xPO_4$ or more complex systems

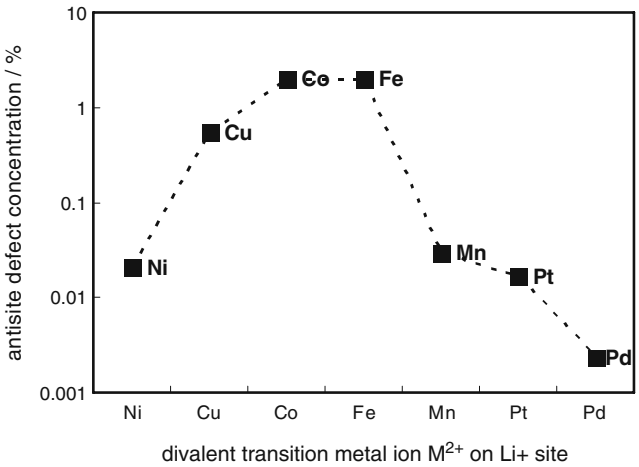

Fig. 2 $Li_M^{/}/M^{\bullet}_{Li}$ antisite defect concentrations predicted for various cations M^{2+} from the BV mismatch analysis assuming an exponential correlation with $\Delta V^2/\mu$ (where μ is the reduced mass of the cation–anion pair) and choosing $c_{antisite}=2\%$ for M=Fe

$LiFe_{1-x-y}Co_xM_yPO_4$ would exhibit a comparable or higher tendency than $LiFePO_4$ for forming antisite defects. In the intensely investigated structures of $LiMnPO_4$ or $LiNiPO_4$, no percolating pathway for Li^+ transport $\perp b$ is formed. The range of M^{2+} cations considered is restricted to transition metal ions that have the potential to compensate for V'_{Li} by a valence change (thereby, e.g., excluding the otherwise matching Zn^{2+}). Any main group cation that exists both in oxidation states 2+ and higher oxidation states would lead to mismatch values exceeding the ones displayed.

On the other hand, the approach described above can also be used to investigate how the tendency for antisite formation and thereby the robustness of the transport pathway can be significantly enhanced by homovalent doping in the case of olivines $LiM_{1-x}X_xPO_4$ with higher M^{2+}/Li^+ antisite defect formation energies such as M=Mn. Chen et al. [21] have recently studied the variation of the rate performance of $LiMn_{0.9}X_{0.1}PO_4$ delithiation as a function of the dopant type X. The BV analysis shows that the tendency for antisite defect formation (expressed by the variation of the reduced mass-scaled BV sum mismatch $\Delta V^2/\mu$) increases in the same sequence X=Mn (i.e., undoped)–Cu–Ni–Mg as the (chemical) delithiation rate as experimentally observed in ref. [21].

Heterogeneous doping by surface modification

In a recent report on extraordinarily high (dis)charging rates of cells based on $LiFePO_4$ with a "fast ion-conducting surface phase through controlled off-stoichiometry" [10, 22], the nominal composition is given as $LiFe_{0.9}P_{0.95}O_{4-d}$. Here, it is assumed—as also suggested by Zaghib et al. [23]—that this effectively leads to phase segregation into $LiFePO_4$ and glassy $Li_4P_2O_7$ (or a nonstoichiometric phase with similar composition) and the effect on the interface between glassy $Li_4P_2O_7$ and $LiFePO_4$ on Li^+ mobility is investigated by MD simulations and BV analysis. Note that, in line with experimental evidence, the electronic transport is assumed to be fast enough to treat all Fe ions as carrying the same fractional charge that accounts for the one V'_{Li} per 96 Li sites. Our MD simulations of bulk $Li_{0.99}FePO_4$ yield results that for the direction $\|b$ are compatible with the experimental anisotropic conductivity studies on single crystals both with regards to absolute values and the activation energy (E_A= 0.57 eV). For a detailed discussion, see Adams S., submitted to *Chemistry of Materials*. The MD simulations of the Li^+ diffusion in the surface-modified $LiFePO_4$ yield (for Li in the $LiFePO_4$ section of the heterostructure) values of $D(Li)_{\|b}$ that are closely similar to the bulk values for $T>700$ K, but nearly two orders of magnitude larger for T=500 K (Fig. 3). No bulk diffusion coefficients could be determined for room temperature values directly from the MD simulations, but a comparison of simulation result for the heterostructure with the extrapolated bulk data suggests a mobility enhancement by more than three orders of magnitude.

In the relaxed MD structure model, it is found for the entire temperature range and for each time step of the respective simulation trajectories that Li^+ ions are significantly enriched on the $LiFePO_4$ side of the interface and depleted on the $Li_4P_2O_7$ glass side (Fig. 4). The overall Li^+ concentration in $LiFePO_4$ is increased by 4–6%. This constitutes a highly significant violation of local electroneutrality in the $LiFePO_4$:

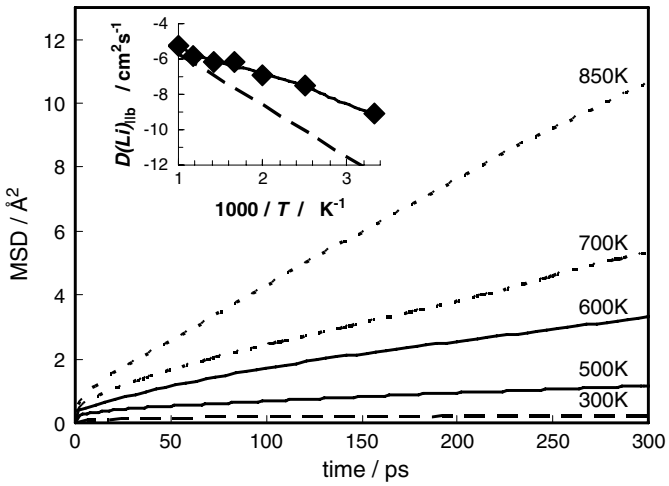

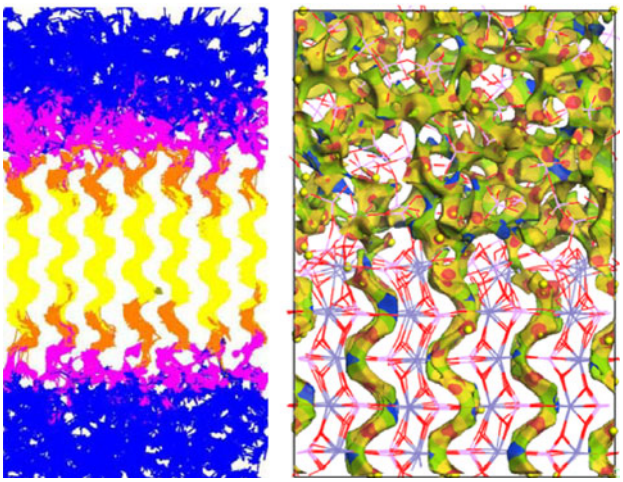

Fig. 3 *l.h.s.* time dependence of mean square displacement (*MSD*) along the *b* direction vs. time for Li^+ ions in the $LiFePO_4$ section of a $LiFePO_4$:$Li_4P_2O_7$ heterostructure at selected temperatures (as indicated in the graph). The *inset* displays an Arrhenius plot of the Li self-diffusion coefficients $D(Li)_{\|b}$ in the $LiFePO_4$ section of the heterostructure, as calculated from the slope of the MSD(time) curves for the temperature range 300 K<T<1,000 K, are shown as an *inset* (*black diamonds*) along with a polynomial fit (*solid line*) and a *broken line* indicating the variation of $D(Li)_{\|b}$ in simulations of bulk $LiFePO_4$ using the same force field. *Center* trace of Li^+ motion over 330 ps from a MD simulation of the heterostructure at T=750 K; *r.h.s.* snapshot of (the BV model of) Li^+ paths in a detail from the same simulation. Isosurface colors (*red*→*blue*) indicate increasing distance to nearest Li

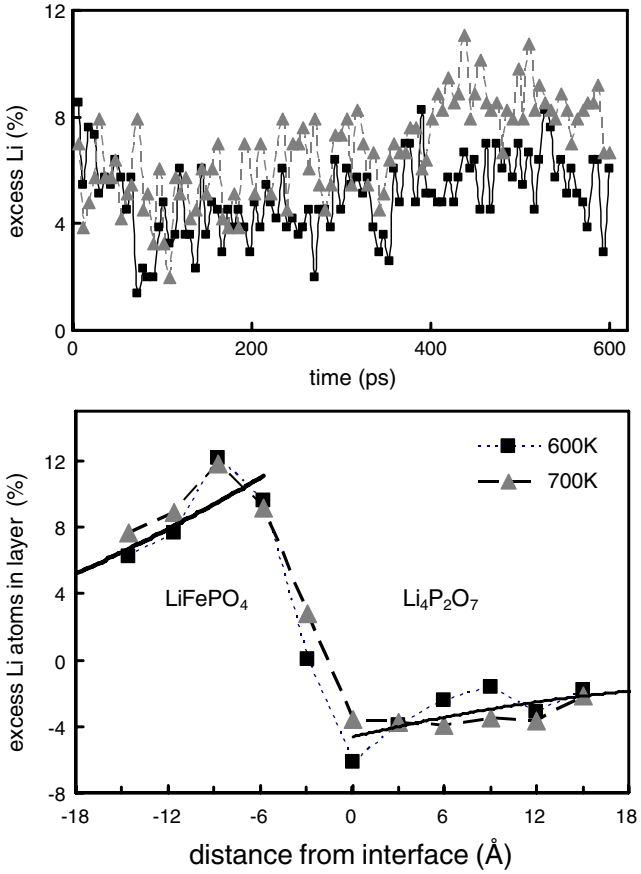

Fig. 4 *Top* percentage of excess Li^+ in the $LiFePO_4$ of a $LiFePO_4$:$Li_4P_2O_7$ heterostructure as a function of time during MD simulation runs at T=600 K and T=700 K. *Bottom* percentage of excess Li^+ in approximately 3 Å thick layers vs. distance from the $LiFePO_4$:$Li_4P_2O_7$ interface averaged over 100 snapshots from NVT MD simulations (*bottom*). *Broken lines* as a guide to the eye, *solid lines* polynomial fits within the $LiFePO_4$ and $Li_4P_2O_7$ phases

$Li_4P_2O_7$ heterostructure, which might imply (1) fast electrostatic energy storage by Li^+ in the interface region and (2) significant potential for enhanced Li^+ ion conductivity by the mesoscopic multiphase effect [24, 25].

A layer-by-layer analysis of the Li^+ displacements in the MD simulations $\|b$ again shows a major enhancement of the overall Li^+ ion mobility in the vicinity of the interface by nearly two orders of magnitude for T=600 K over the simulated bulk values at the same temperature (Fig. 5). At 600 K, the relative enhancement is most pronounced on the $LiFePO_4$ side of the interface, but the maximum of the lithium self-diffusion coefficient $D(Li)_{\|b}$ occurs on the phosphate glass side of the interface, implying that the Li redistribution also enhances the "vacancy" concentration in the glassy surface layer. Closer to room temperature, the maximum of the diffusion coefficient is shifted to the $LiFePO_4$ side of the interface. The anisotropy of the Li^+ diffusion coefficient $\|b/\perp b$ is reduced from >1,000 in the bulk of the $LiFePO_4$ to (trivially) one within the glass phase; at the interface, the motion perpendicular to the interface even seems to be slightly preferred. The observed reduction of the anisotropy involves both the spontaneous formation of antisite pairs (that as discussed above connect Li^+ channels $\perp b$) in the vicinity of the interface and Li^+ migration pathways across the interface. Overall, this will help to ensure a balancing of the Li content in the one-dimensional channels of the respective Li_xFePO_4 phases and should also accelerate the propagation of the $Li_{1-x}FePO_4$:$Li_{0+y}FePO_4$ interface along the a direction perpendicular to the channels [26, 27] during charging or discharging. The study is continued to include a wider range of nominal lithium contents in order to clarify the extent of defect concentration/distribution and heterointerface effects on the dimensionality and rate of the complex size-dependent phase transformation and transport properties in this system during Li^+ (de) insertion.

Summary

BV models clarify how seemingly conflicting findings on the Li^+ pathway dimensionality in $LiFePO_4$ and related olivines can be reconciled, taking into account the effect of antisite defects on long-range mobility. Surface modification of $LiFePO_4$ nanocrystals by a $Li_4P_2O_7$ glass surface leads to a significant heterogeneous doping effect enhancing the Li^+ ion mobility. Moreover, the enhanced mobility perpendicular to the Li channels should facilitate a fast charging or discharging of Li batteries with such surface-modified LFP electrodes.

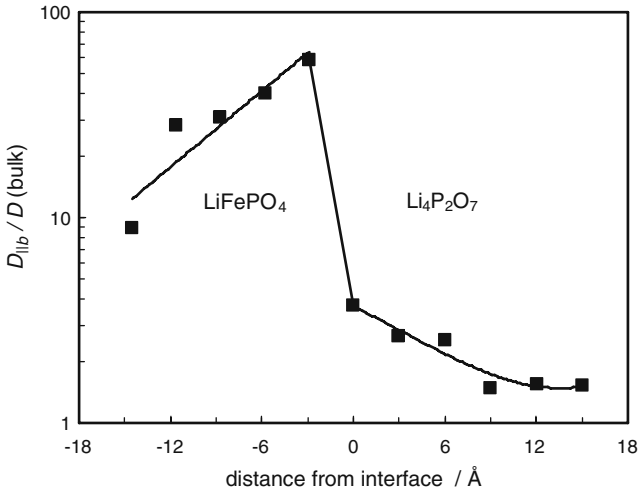

Fig. 5 Variation of the relative enhancement of the Li^+ diffusion coefficient $\|b$ in the vicinity of the modeled $LiFePO_4$:$Li_4P_2O_7$ interface (with respect to values of $D_{\|b}$ for the respective bulk phase) with the distance from the interface. Data are based on a 600-ps trajectory from the NVT MD simulations at T=600 K

Acknowledgements The financial support by A*Star (NSF/SERC Materials World Network 062 119 0009) is gratefully acknowledged.

References

1. Islam MS, Driscoll DJ, Fisher CAJ, Slater PR (2005) Chem Mater 17:5085–5092
2. Maxisch T, Zhou F, Ceder G (2006) Phys Rev B 73:104301
3. Ouyang C, Shi S, Wang Z, Huang X, Chen L (2004) Phys Rev B 69:104303
4. Adams S (2006) J Power Sources 159:200–204
5. Streltsov VA, Belokoneva EL, Tsirelson VG et al (1993) Acta Crystallogr B Struct Sci 49:147–153
6. Nishimura SI, Kobayashi G, Ohoyama K, Kanno R, Yashima M, Yamada A (2008) Nat Mater 7:707–711
7. Amin R, Maier J (2008) Solid State Ion 178:1831–1836
8. Amin R, Maier J, Balaya P, Chen DP, Lin CT (2008) Solid State Ion 179:27–32
9. Li J, Yao W, Martin S, Vaknin D (2008) Solid State Ion 179:2016–2019
10. Kang B, Ceder G (2009) Nature 458:190–193
11. Adams S, Prasada Rao R (2009) Phys Chem Chem Phys 11:3210–3216
12. Gale JD (1997) J Chem Soc Faraday Trans 93:629–637
13. Materials Studio 4.4 (2008) Accelrys Inc., San Diego, CA, pp 92121–3752
14. Adams S (2004) softBV 0.96. Available at http://www.softBV.net
15. Fisher CAJ, Prieto VMH, Islam MS (2008) Chem Mater 20:5907–5915
16. Gibot P, Casa-Cabanas M, Laffont L, Levasseur S et al (2008) Nat Mater 7:741–747
17. Hamelet S, Gibot P, Casas-Cabanas M, Bonnin D et al (2009) J Mater Chem 19:3979–3991
18. Chen J, Wittingham MS (2006) Electrochem Commun 8:855–858
19. Chung SY, Yamamoto SYT, Ikuhara Y (2008) Phys Rev Lett 100:125502
20. Axmann P, Stinner C, Wohlfahrt-Mehrens M, Mauger A, Gendron F, Julien CM (2009) Chem Mater 21:1636–1644
21. Chen G, Wilcox JD, Richardson TD (2008) Electrochem Solid State Lett 11:A190–A194
22. Ceder G, Kang B (2009) J Power Sources 194:1024–1028
23. Zaghib K, Goodenough JB, Mauger A, Julien C (2009) J Power Sources 194:1021–1023
24. Maier J (2005) Nat Mater 4:805–815
25. Maier J (2009) Adv Mater 21:2571–2585
26. Chen GY, Song XY, Richardson TJ (2006) Electrochem Solid State Lett 9:A295–A298
27. Delmas C, Maccario M, Croguennec L, Le Cras F, Weill F (2008) Nat Mater 7:665–671